Progress In Electromagnetics Research M, Vol. 59, 203–212, 2017

An Efficient Adaptive Clutter Compensation Algorithm for Bistatic Airborne Radar Based on Improved OMP Application

Cunxiao Ji[1, 2, *], Mingwei Shen[1, 2], Chao Liang[2], Di Wu[3], and Daiyin Zhu[3]

Abstract—In this study, the misalignment of bistatic clutter spectral centers is considered, and an efficient adaptive main-lobe clutter compensation approach is presented for mitigating the bistatic geometry-induced clutter dispersion. In order to reduce computational load, an improved orthogonal matching pursuit (OMP) is introduced into the space-time clutter spectrum estimation. This method can accurately extract the required parameters for compensating the clutter spectral centers misalignment via sparse reconstruction with the desired Doppler cells. Simulation results are presented to demonstrate the effectiveness and efficiency of the proposed method.

1. INTRODUCTION

Several research activities are in progress on bistatic radar systems for airborne applications in recent years. Bistatic airborne radar systems offer several advantages over their monostatic counterparts, including far range coverage, strong anti-interference and high security capability. Since the transmitter (TX) and receiver (RX) motions yields a non-stationary behavior of the clutter spectrum, a bistatic airborne radar system must effectively cope with severe spectrally diverse clutter returns.

Brennan and Reed proposed a concept of space-time adaptive processing (STAP) [1, 2] in 1973, which can improve the monostatic airborne radar moving target detection performance remarkably. STAP has become an advanced technique and is considered as a powerful tool for monostatic airborne radar detecting moving target and suppressing ground clutter. However, it is difficult to apply the STAP approach to bistatic airborne radar in practice because of strong non-stationary behavior of the clutter spectrum [3].

In the last few years, a number of contributions have been proposed, and the problem of clutter range dependence is largely addressed. Among them, there are some effective approaches to limit the effect of monostatic clutter range dependence such as Doppler wrapping (DW) [4], angle-Doppler compensation (ADC) [5, 6], and adaptive angle-Doppler compensation (AADC) [7]. An extension of AADC algorithm for bistatic STAP is also presented [8] to compensate for the spectral centre (SC) misalignment and angel-Doppler trajectory slope variability over range. However, the compensation parameters of DW and ADC are sensitive to system error. The required parameters of the AADC and adaptive FO-ADC approach are obtained by the minimum variance (MV) estimation of the clutter spectrum using a sub-aperture smoothing approach, which results in a great increase of computational load and limits real-time processing.

In this paper, an improved OMP [9] approach is employed to obtain both main-lobe clutter spectrum estimation and the required compensation parameters for clutter SC. It is shown that the

Received 8 June 2017, Accepted 15 August 2017, Scheduled 22 August 2017

* Corresponding author: Cunxiao Ji (hhujcx@yeah.net).

[1] College of Computer and Information Engineering, Hohai University, Nanjing 211100, China. [2] Science and Technology on Electronic Information Control Laboratory, Chengdu 610036, China. [3] Key Laboratory of Radar Imagine and Microwave Photonics & Ministry of Education, Nanjing University of Aeronautics and Astronautics, Nanjing 210016, China.

SC can be estimated accurately from the data themselves. In contrast to the reduced-dimension sparse reconstruction (RDSR) [10–12], the presented method can significantly reduce the computational load.

The rest of this paper is organized as follows. In Section 2, we first analyze the range dependence clutter dispersion of bistatic airborne radar system. Section 3 is devoted to the clutter spectrum sparse reconstruction using the improved OMP and the main-lobe clutter compensation. The validity of the method is confirmed by the simulation experiment in Section 4. Finally, a brief conclusion is drawn in Section 5.

2. PROPERTIES OF BISTATIC AIRBORNE RADAR CLUTTER

The receiving system under consideration is a pulse Doppler radar residing on an airborne platform. The RX antenna is a uniform linear array (ULA), which consists of N elements with inter-element spacing d. Each of these elements receives K echoes from a transmitted train of K coherent pulses during the coherent processing interval (CPI) with wavelength λ and pulse repetition frequency (PRF). The TX and RX platforms are at the altitudes of H_t and H_r, and v_t and v_r are the TX and RX platforms' speeds, respectively.

Without loss of generality, the bistatic airborne radar geometry is shown in Fig. 1. The coordinate system is assumed that the x-axis is aligned with the RX flight direction; β_2 represents the TX flight direction; points O and Q stand for the projections of the RX and TX on the ground with distance D_{tr}; β_1 represents the angle between OQ and x-axis. Point P stands for one scatterer in the scenario of interest; R_t is the distance between TX and P; R_r is the distance between RX and P, respectively. We assume that the TX and RX work in sync for the convenience of using STAP technology. For the convenience of discussion, in this article, we deal with only one such configuration $\beta_1 = \beta_2 = 0$.

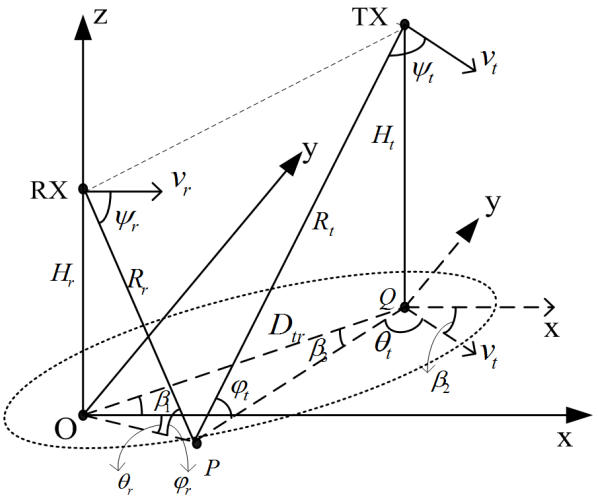

Figure 1. Geometry of bistatic airborne radar.

As well known, the Doppler frequency associated to each scatterer is only dependent on the scatterer position and the antenna geometry and motion [1]. In the case of a bistatic airborne radar system, the clutter trajectory [3] in angle-Doppler domain can be given by:

$$f_d = \frac{v_t}{\lambda}\cos\theta_t\cos\varphi_t + \frac{v_r}{\lambda}\cos\theta_r\cos\varphi_r \tag{1}$$

where θ_t and φ_t represent TX azimuth angle and elevation angle, and θ_r and φ_r represent RX azimuth angle and elevation angle, respectively. For the main-lobe clutter, we assume that $\theta_{t_{main}} = \frac{\pi}{2}$, so that formula (1) can be simplified to the formula below:

$$f_d = \frac{v_r}{\lambda}\cos\theta_{rmain}\cos\varphi_{rmain} \tag{2}$$

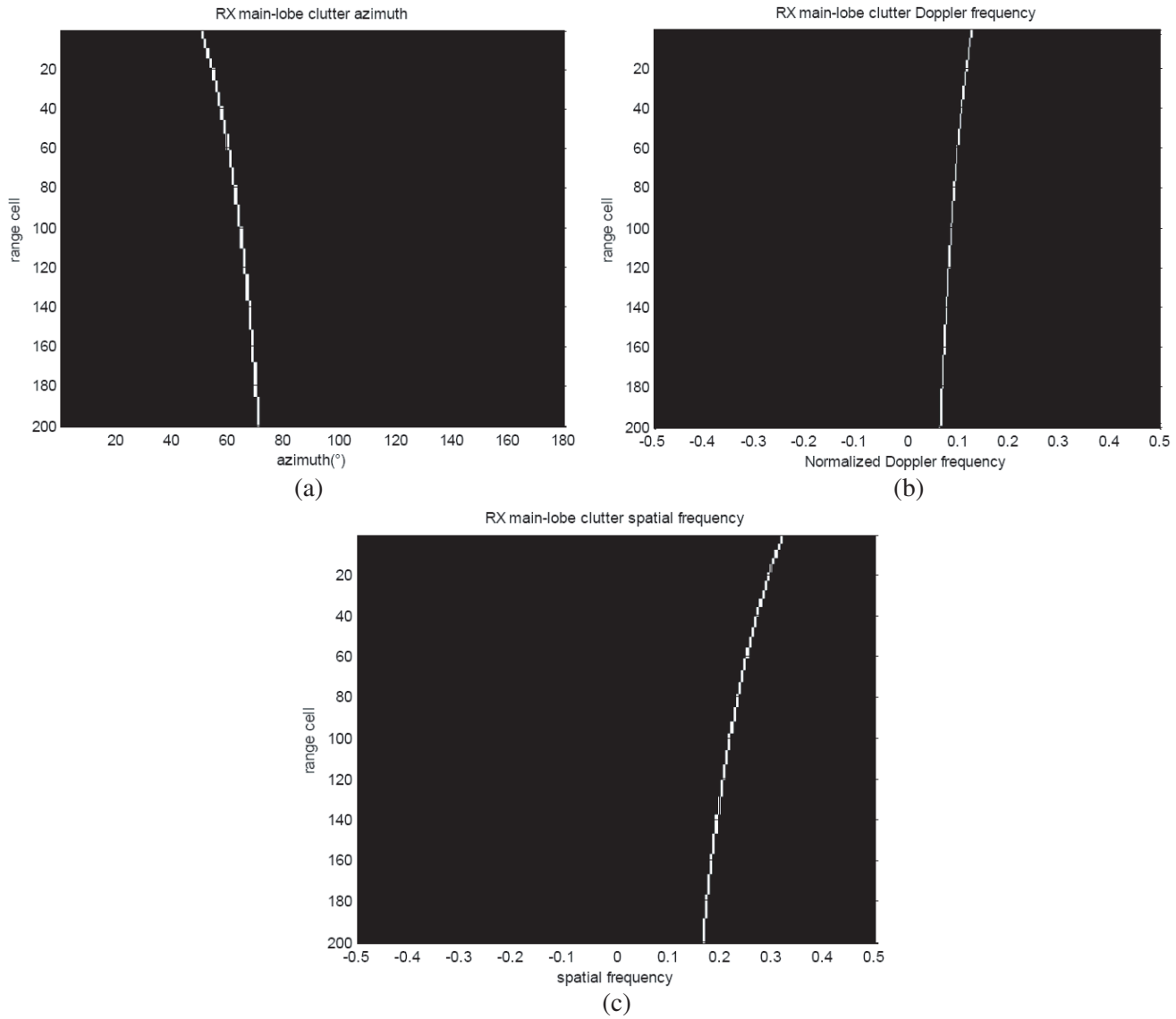

Figure 2. θ_{rmain}, Doppler frequency and spatial frequency in different range cells. (a) θ_{rmain}. (b) Doppler frequency. (c) Spatial frequency.

Considering $N = 16$ elements and $K = 64$ pulses in one CPI, for the RX, the trajectories of θ_{rmain}, Doppler frequency and spatial frequency corresponding to 200 range cells are depicted in Fig. 2(a), Fig. 2(b) and Fig. 2(c). It is apparent that $\theta_{t_{main}}$ and θ_{rmain} do not overlap, θ_{rmain} varies fast in short-range clutter area. In remote areas, the trend is slow. The Doppler frequency and spatial frequency of the RX main-lobe clutter vary with range cells as well. The bistatic airborne clutter is range dependence non-stationary.

3. ESTIMATION OF MAIN-LOBE CLUTTER SPECTRUM AND SC COMPENSATION

From the above statement, we can see that the bistatic airborne radar range dependence clutter dispersion leads to two-dimensional clutter spectrum broadening seriously, which decreases the subsequent STAP performance for slow-moving target detection. In this section, we present an improved OMP approach to significantly reduce the complexity of the compensation parameter estimation used in

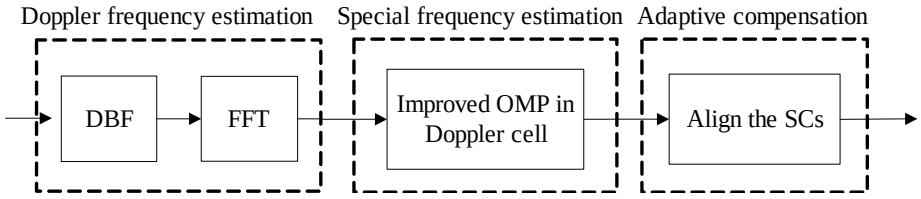

Figure 3. The EAADC flowchart.

AADC. With reference to [11, 12], the implementation of the presented efficient adaptive angle-Doppler compensation (EAADC) strategy is summarized in the following steps and sketched in Figure 3.

3.1. Estimation of Main-Lobe Clutter Doppler Frequency

The received data $\mathbf{X}_l$ from the N-element array for the l-th range gate can be reshaped into a $N \times K$ matrix as

$$\mathbf{X}_l = [\ \mathbf{S}_{l\_1} \quad \mathbf{S}_{l\_2} \quad \cdots \quad \mathbf{S}_{l\_K}\ ]_{N\times K} \tag{3}$$

where $\mathbf{S}_{l\_i}$ represents the spatial snapshot vector from the N-element array for the l-th pulse of a K-pulse CPI. The received sum beam output can be derived via digital beam forming (DBF) and can be transformed to the Doppler domain via Fourier Transform, which can be implemented as

$$\mathbf{D}_{\Sigma,l} = \mathbf{w}_{\Sigma,l}\mathbf{X}_l\mathbf{F}_{\Sigma,D}^H = [\ \mathbf{D}_{\Sigma,l\_1} \quad \mathbf{D}_{\Sigma,l\_2} \quad \cdots \quad \mathbf{D}_{\Sigma,l\_K}\ ] \tag{4}$$

where $\mathbf{w}_{\Sigma,l}$ denotes the spatial weight of sum beam; $\mathbf{F}_{\Sigma,D}$ comprises the Fourier Transform weights; the superscript $(^H)$ denotes complex conjugate transpose; $\mathbf{D}_{\Sigma,l\_i}$ represents the output of the i-th sum beam Doppler cell. As a consequence, the main-lobe clutter Doppler frequency can be determined by the peak value of $\mathbf{D}_{\Sigma,l}$.

3.2. Estimation of Main-Lobe Clutter Spatial Frequency

If we still utilize fast Fourier Transformation (FFT) to obtain the angle spectrum in the spatial domain, the bistatic clutter spectrum will suffer from main-lobe broadening, high side-lobe leakage, etc., which consequently lead to a poor estimation of the spatial frequency. To obtain high-resolution spectral estimation, sparse reconstruction (SR) is utilized to estimate the clutter spectrum. However, the implementation of SR in the angle-Doppler domain requires complex multiplications [13, 14], which is impractical. Compared with two-dimensional SR in the angle-Doppler domain, an RDSR algorithm was proposed in [11, 12], and the RDSR based on convex optimization also has a high computational cost, which limits its real-time processing.

In this paper, an improved OMP technique is utilized to reduce the computational load, and only the array output corresponding to the main-lobe clutter is recovered in the spatial domain. Therefore, the angle spectrum can be achieved:

$$\begin{cases} \hat{\boldsymbol{\sigma}}_{l\_i,\max} = \operatorname{argmin} \|\boldsymbol{\sigma}_{l\_i,\max}\|_1 \\ s.t. \quad \|\mathbf{D}_{l\_i,\max} - \mathbf{M}_i\boldsymbol{\sigma}_{l\_i,\max}\|_2 \le \delta_i \end{cases} \tag{5}$$

where $\|\cdot\|_1$ stands for the L_1 norm, $\|\cdot\|_2$ the L_2 norm, $\mathbf{D}_{l\_i,\max}$ the Doppler-element data corresponding to the maximum Doppler cell of the l-th range gate, $\boldsymbol{\sigma}_{l\_i,\max}$ the estimated clutter distribution response in spatial domain, $\mathbf{M}_i$ an over complete basis representation in terms of all possible sources locations, $\boldsymbol{\mu}_j$ the j-th column of $\mathbf{M}_i$, and δ_i the error allowance related to $\mathbf{D}_{l\_i,\max}$.

The flowchart of the improved OMP is shown in Fig. 4 for the maximum Doppler cell of the l-th range gate. To apply the OMP with the unknown sparsity situation, firstly the initial value S_l of the sparsity is set to 1. Then the column $\boldsymbol{\mu}_j$, which has the max-relativity with the residual vector $\mathbf{r}_t$, is selected from $\mathbf{M}_i$:

$$\boldsymbol{\mu}_{j_t} = \arg\max_{\mu_j} |\langle \mathbf{r}_{t-1}, \boldsymbol{\mu}_j \rangle|_{j=1,2,\ldots,N_s} \tag{6}$$

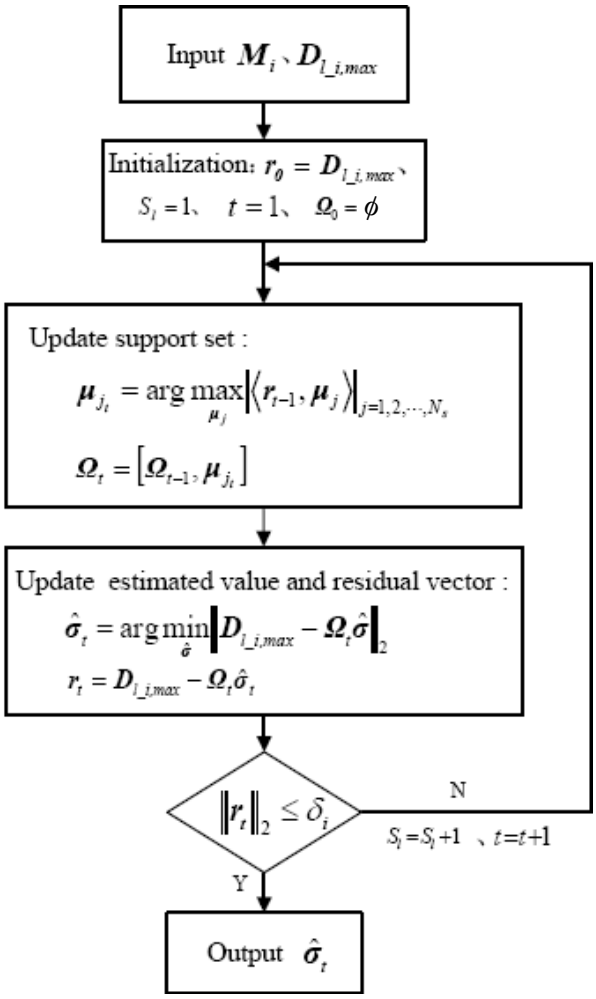

Figure 4. Flowchart of the improved OMP algorithm.

Sequentially we can obtain the corresponding support set $\mathbf{\Omega}_t = [\mathbf{\Omega}_{t-1}, \boldsymbol{\mu}_{j_t}]$. Consequently, the scattering coefficients of main-lobe clutter spectrum can be recovered efficiently, and the residual vector can be updated as follows:

$$\begin{aligned} \hat{\boldsymbol{\sigma}}_t &= \arg\min_{\sigma} \|\mathbf{D}_{l\_i,\max} - \mathbf{\Omega}_t \boldsymbol{\sigma}_t\|_2 = \left(\mathbf{\Omega}_t^H \mathbf{\Omega}_t\right)^{-1} \mathbf{\Omega}_t^H \mathbf{D}_{l\_i,\max} \\ \mathbf{r}_t &= \mathbf{D}_{l\_i,\max} - \mathbf{\Omega}_t \hat{\boldsymbol{\sigma}}_t \end{aligned} \tag{7}$$

The reconstruction process ends when $\|r_t\|_2 \le \delta_i$. Otherwise, S_l will increase and continue iterating, and finally, the value of the sparsity is $S_{l,\max}$ by the end of the reconstruction process. Applying this procedure repeatedly for all L range gates, we can obtain the high-resolution two-dimensional (2D) spectral distribution of the bistatic main-lobe clutter. Due to the spectrum discontinuity of SR via the improved OMP in the spatial domain, the spectral centre frequency estimation method in the reference [15] is also employed to obtain the peak of main-lobe clutter in spatial domain.

3.3. Adaptive Compensation of the Spectral Centers

AADC is an effective approach to directly align SCs over range. Therefore, the range dependent SCs of the 2D spectrum now can be effectively removed, since the Doppler and spatial frequencies of the bistatic main-lobe clutter have already been estimated in Sections 3.1 and 3.2, respectively.

We assume that the estimated SC of the reference range cell is (f_{s_0}, f_{d_0}), and the SC of the l-th range cell is (f_{s_l}, f_{d_l}). The SC displacements in terms of the spatial frequency Δf_{s_l} and normalized Doppler frequency Δf_{d_l} are as follows:

$$\Delta f_{s\_l} = f_{s\_l} - f_{s\_0} \tag{8}$$

$$\Delta f_{d\_l} = f_{d\_l} - f_{d\_0} \tag{9}$$

We can apply a complex linear phase taper over both angle and Doppler dimensions to compensate for the SC migration, which can be expressed as

$$\mathbf{C}_l = \mathbf{T}_{s\_l}\mathbf{X}_l\mathbf{T}_{t\_l} \tag{10}$$

where $\mathbf{T}_{s\_l}$ and $\mathbf{T}_{t\_l}$ are the compensation factor in the spatial domain and compensation factor in the Doppler domain, respectively. They can be expressed as:

$$\mathbf{T}_{s\_l} = \begin{bmatrix} 1 & 0 & \dots & 0 \\ 0 & \exp\left(j2\pi\Delta f_{s\_l}\right) & \dots & 0 \\ \vdots & \vdots & \vdots & \vdots \\ 0 & 0 & \dots & \exp\left(j2\pi\left(N-1\right)\Delta f_{s\_l}\right) \end{bmatrix} \tag{11}$$

$$\mathbf{T}_{t\_l} = \begin{bmatrix} 1 & 0 & \dots & 0 \\ 0 & \exp\left(j2\pi\Delta f_{d\_l}\right) & \dots & 0 \\ \vdots & \vdots & \vdots & \vdots \\ 0 & 0 & \dots & \exp\left(j2\pi\left(K-1\right)\Delta f_{d\_l}\right) \end{bmatrix} \tag{12}$$

The STAP performance can be significantly improved owing to the reduction of the bistatic clutter dispersion by applying the aforementioned implementation to the secondary data before covariance estimation. The improvement factor (IF), given as the ratio of output SINR to the input SINR, is presented to evaluate the effectiveness of the proposed method as well as the performance of the mitigating the bistatic clutter dispersion with a reduced-dimension (RD) STAP approach [16]. The detailed analysis will be given in Section 4.

4. SIMULATION RESULTS AND ANALYSIS

This section is devoted to illustrating the performance of the fast implementation of spectral estimation via improved OMP and clutter compensation for bistatic airborne radar using the simulated data. In the simulation, consider RX antenna with $N = 16$ elements and $K = 64$ pulses in one CPI. The bistatic airborne radar system parameters are listed in Table 1.

Table 1. Simulation parameters for bistatic airborne radar.

PRF f_r	4200 Hz
Bandwidth f_s	2 MHz
Element spacing and wavelength ratio	0.5
TX platform height H_t	10 km
RX platform height H_r	6 km
The distance D_{tr}	10 km
TX main-lobe θ_{tmain}	0.5π
The angle β_1	0
The angle β_2	0
TX Platform velocity v_t	150 m/s
RX Platform velocity v_r	200 m/s

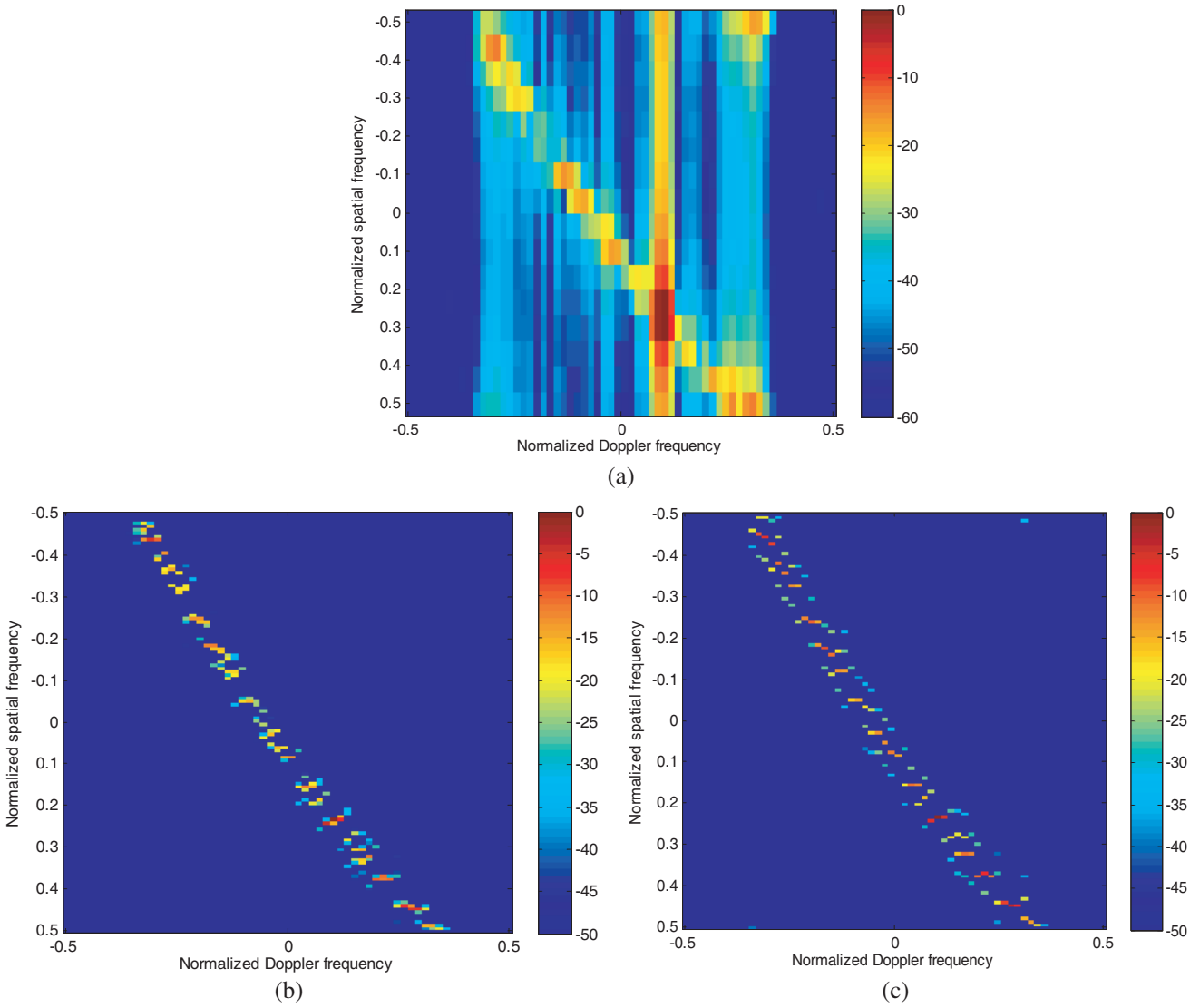

Figure 5. The clutter angle-Doppler spectrum image of the 150th range cell. (a) 2D FFT. (b) Spatial RDSR. (c) Improved OMP.

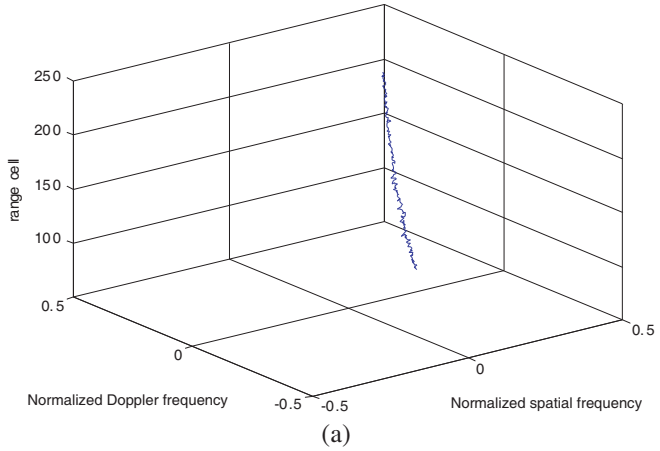

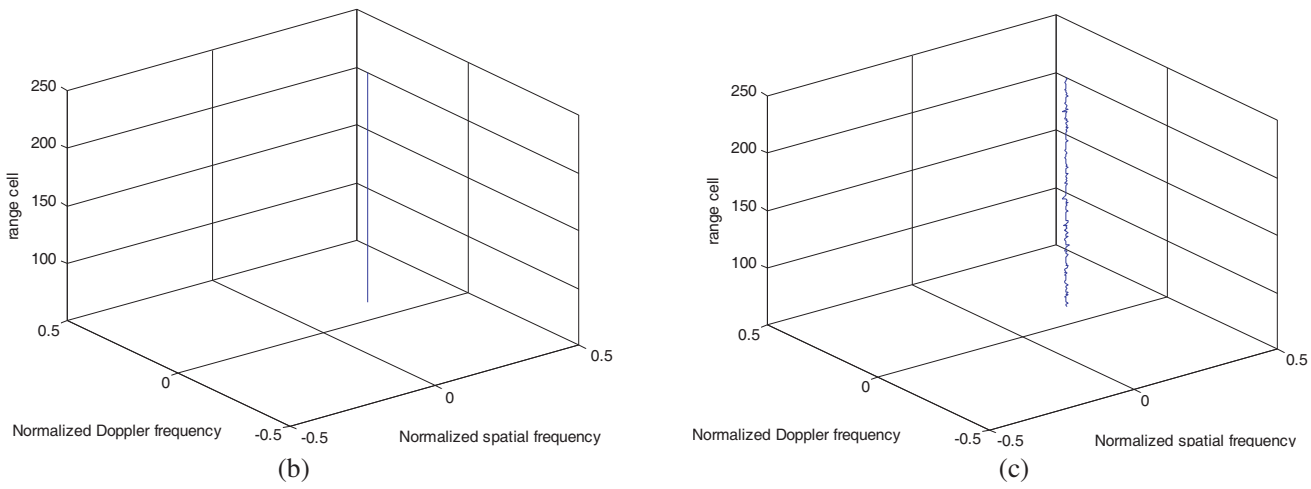

Figure 6. SCs migration over range. (a) Before compensation. (b) RDSR with AADC. (c) Improved OMP with AADC.

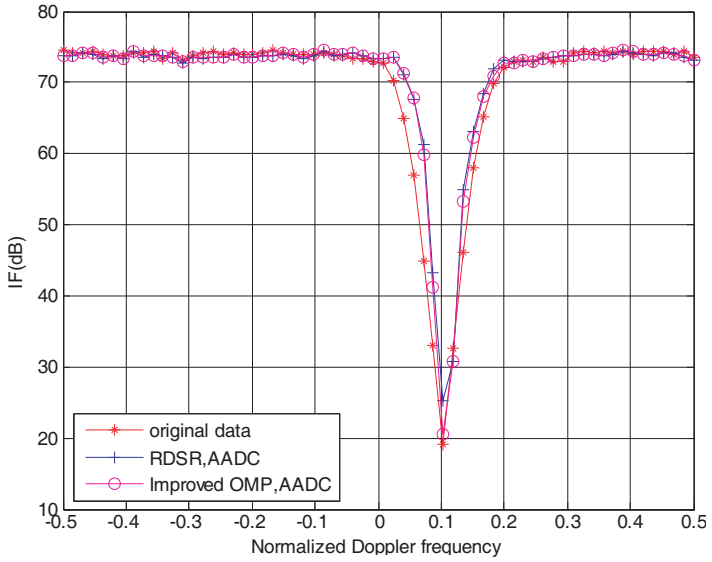

Figure 7. IF of the RD STAP after compensation.

The bistatic spectrum obtained via 2D FFT of the 150th range cell is shown in Fig. 5(a). To evaluate the performance of the improved OMP in the spatial domain, the angle-Doppler spectrum obtained by using the improved OMP in each Doppler cell with the simulation parameter $\delta_i = \frac{1}{10}\|D_{l\_i,\max}\|_2$ is shown in Fig. 5(c). For comparison purpose, the sparse reconstructed spectrum obtained via RDSR is also provided in Fig. 5(b). It is clear that Fig. 5(b) has much better resolution than Fig. 5(c). However, Fig. 5(c) has much better resolution and lower side-lobe level than that of 2D FFT as well, which will also improve the accuracy of estimating the SC location of bistatic main-lobe clutter.

In the simulation, the 150th range cell is selected to be the reference cell, and the range cells from 1 to 250 are compensated based on the reference cell SC. The SCs migrations over range are depicted in Fig. 6. It can be seen that the bistatic clutter SCs before compensation are misaligned over range due to bistatic configuration. The bistatic clutter spectrum SCs after realignment are depicted in Fig. 6(b) using RDSR in conjunction with the AADC. Fig. 6(c) shows the bistatic clutter spectrum SCs after realignment using the improved OMP in conjunction with the AADC. It is apparent that the bistatic range dependence clutter dispersion has been significantly mitigated after main-lobe compensation, and

the SCs of the spectral traces are exactly co-located.

Figure 7 presents the IF curves obtained after applying the improved OMP and the RDSR in conjunction with AADC approach to the secondary data, where the 150th range cell is selected as the reference cell. Two SR methods together with AADC yield reduced bistatic clutter power dispersion with respect to the case of without compensation. Thus, an improvement of 6.04 dB and 6.58 dB can achieved around SC after compensation, respectively.

To complete our analysis, the complex multiplications of bistatic main-lobe clutter spectrum estimation using RDSR and the improved OMP are calculated. For L range cells bistatic main-lobe clutter spectrum estimation, the former is about $O[N_s^2NL]$ while the latter is about $\sum_{l=1}^{L} O[N_sN\frac{S_{l,\max}(1+S_{l,\max})}{2}]$, where $N_s = \rho_s N$ and considering the angle resolution scale $\rho_s = 8$. From the simulation, the average $S_{l,\max}$ of all L range cells is about $S_l = 4$, so the total complex multiplications for the improved OMP implementation is $O[N_sN\frac{S_l(1+S_l)}{2}L]$. In consequence, the complex multiplications for the improved OMP in this paper is significantly better than that for the RDSR since the former is about 7.81% of the latter. It can be found that the improved OMP together with AADC offers a good tradeoff between SCs compensation and complex multiplications. These two methods with AADC usually yield comparable performance, with one of them being definitely the best one.

5. CONCLUSION

This work describes an improved EAADC to mitigate the range dependence clutter dispersion for bistatic airborne radar system. We use the improved OMP method to calculate the requisite spatial frequency within the main-lobe clutter Doppler cells for realigning the spectral center instead of the RDSR, so the complex multiplications is dramatically reduced. The performance of the EAADC has been demonstrated against synthetic data showing that this method offers a good tradeoff between SCs compensation and complex multiplications. Therefore, this method is more suitable for bistatic airborne radar real-time processing.

ACKNOWLEDGMENT

This work was supported in part by the National Natural Science Foundation of China (No. 61201459, No. 61301212), Science and Technology on Electronic Information Control Laboratory and China Scholarship Council (No. 201606715009).

REFERENCES

1. Klemm, R., *Principles of Space-time Adaptive Processing*, 1–116, The Institution of Electrical Engineers, London, United Kingdom, 2002.
2. Brennan, L. E. and I. S. Reed, "Theory of adaptive radar," *IEEE Transactions on Aerosp. Electron. Syst.*, Vol. 9, No. 2, 237–252, Mar. 1973.
3. Meng, X. D., J. X. Wu, T. Wang, et al., "Clutter analysis and range-ambiguous clutter suppression for bistatic airborne radar," *Journal of Xidian University*, Vol. 35, No. 6, 992–998, 2008.
4. Borsari, G. K., "Mitigating effects on STAP processing caused by an inclined array," *Proceedings of the Radar Conference, 1998, Radarcon 98*, 135–140, IEEE, 1998.
5. Zhao, J. and Z. D. Zhu, "A multiple space angle compensation method for airborne radar with non-side-looking uniform linear array," *Acta Aeronaut Astronaut Sin*, Vol. 31, No. 11, 2216–2221, 2010.
6. Fallah, A. and H. Bakhshi, "Extension of Adaptive Angle-Doppler Compensation (AADC) in STAP to increase homogeneity of data in airborne bistatic radar," *Sixth International Symposium on Telecommunications*, 367–372, IEEE, 2013.
7. Tian, B., D. Y. Zhu, and Z. D. Zhu, "A fast adaptive angle Doppler compensation method," *Acta Aeronaut Astronaut Sin*, Vol. 32, No. 9, 1705–1713, 2011.

8. Colone, F., "Spectral slope-based approach for mitigating bistatic space-time adaptive processing clutter dispersion," *IET Radar Sonar & Navigation*, Vol. 5, No. 5, 593–603, 2011.
9. Wang, J., S. Kwon, and B. Shim, "Generalized orthogonal matching pursuit," *Mathematics*, Vol. 60, No. 12, 6202–6216, 2014.
10. Shen, M. W., J. Wang, D. Wu, et al., "An efficient data domain STAP algorithm based on reduced-dimension sparse reconstruction," *Acta Electronica Sinica*, Vol. 42, No. 11, 2286–2290, 2014.
11. Shen, M. W., J. Yu, D. Wu, et al., "An efficient adaptive angle-doppler compensation approach for non-sidelooking airborne radar STAP," *Sensors*, Vol. 15, No. 6, 13121–13131, 2015.
12. Wang, J., M. W. Shen, D. Wu, et al., "An efficient STAP algorithm for nonsidelooking airborne radar based on mainlobe clutter compensation," *Journal of Radars*, Vol. 3, No. 2, 235–240, 2014.
13. Wu, H. and S. Wang, "Adaptive sparsity matching pursuit algorithm for sparse reconstruction," *IEEE Signal Processing Letters*, Vol. 19, No. 8, 471–474, 2012.
14. Gurbuz, A. C., V. Cevher, and J. H. Mcclellan, "Bearing estimation via spatial sparsity using compressive sensing," *IEEE Transactions on Aerospace & Electronic Systems*, Vol. 48, No. 2, 1358–1369, 2012.
15. Wu, H., Y. L. Wang, and J. W. Chen, "Nonhomogeneous detector for STAP based oil spectral center frequency method," *Journal of Systems Engineering and Electronics*, Vol. 30, No. 4, 606–608, 2008.
16. Wang, Y. L., Y. N. Peng, and Z. Bao, "Space-time adaptive processing for airborne radar with various array orientations," *IEE Proceedings — Radar, Sonar and Navigation*, Vol. 144 No. 6, 330–340, 1997.